

DETECTION OF A CORRUGATED VELOCITY PATTERN IN THE SPIRAL GALAXY NGC 5427¹

EMILIO J. ALFARO,² ENRIQUE PÉREZ,² ROSA M. GONZÁLEZ DELGADO,² MARCO A. MARTOS,³ AND JOSÉ FRANCO³

Received 2000 June 26; accepted 2000 November 14

ABSTRACT

Here we report the detection, in H α emission, of a radial corrugation in the velocity field of the spiral galaxy NGC 5427. The central velocity of the H α line displays coherent, wavy-like variations in the vicinity of the spiral arms. The spectra along three different arm segments show that the maximum amplitude of the sinusoidal line variations are displaced some 500 pc from the central part of the spiral arms. The peak blueshifted velocities appear some 500 pc upstream of the arm, whereas the peak redshifted velocities are located some 500 pc downstream of the arm. This kinematical behavior is similar to the one expected in a galactic bore generated by the interaction of a spiral density wave with a thick gaseous disk, as recently modeled by Martos & Cox.

Subject headings: galaxies: individual (NGC 5427) — galaxies: kinematics and dynamics — galaxies: spiral — galaxies: structure

1. INTRODUCTION

It has been known for decades that the gaseous disk of our Galaxy displays coherent vertical distortions (Kerr 1957; Gum, Kerr, & Westerhout 1960). In particular, for locations inside the solar circle, a wavy structure has been observed in the vertical distribution of several interstellar tracers including the atomic and ionized components (Lockman 1977; Sanders, Solomon, & Scoville 1984; Spicker & Feitzinger 1986; Malhotra 1995) and young stellar objects (see, e.g., Dixon 1967; Alfaro et al. 1992a, 1992b; Berdnikov & Efremov 1993). These undulations, distributed above and below the mean Galactic plane and in both the azimuthal and radial directions, have been termed “corrugations,” and they seem to be common features appearing in disk galaxies. They have also been detected in both the gaseous and stellar disks of other spiral galaxies such as M31 (Arp 1964), NGC 4244, and NGC 5023 (Florido et al. 1991).

Their origin could be ascribed to either well-localized features, such as spiral arms and collisions with high-velocity clouds (HVCs), or large-scale perturbations, such as gravitational interactions. For instance, some authors have explored the possibility of undulations along spiral arms, induced by magneto-gravitational instabilities (see, e.g., Nelson 1985; Gómez de Castro & Pudritz 1992; Kim, Hong, & Ryu 1997; J. Franco et al. 2001, in preparation). In this case, the arms are corrugated by the undular mode (Parker 1966) of the instability, and the structuring occurs *only* in the azimuthal direction (a possible association to the radial patterns could be made if one assumes that these are the projection of the azimuthal corrugations on the radial direction). Another localized origin could be ascribed to collisions of HVC with the disk of a galaxy; HVC impacts could cause the midplane disk to oscillate in a mode of

wavy patterns as well (Franco et al. 1988; Santillán et al. 1999). In the large-scale scenario, the undulations represent the natural response of the disk, which behaves like a loose drumhead, to the perturbations induced by either some companion galaxies or other galactic subsystems (Weinberg 1991; Edelsohn & Elmegreen 1997).

One obvious inference is that these corrugations should be associated with equally undulated coherent motions, and models addressing the vertical displacements also show wavelike z -velocity fields with amplitudes of the order of tens of km s⁻¹ (see, e.g., Nelson 1976, 1985; Franco et al. 1988, 2001, in preparation; Edelsohn & Elmegreen 1997; Kim et al. 1997; Santillán et al. 2000). Despite this expectation, however, the data about actual velocity features associated with spatial corrugations are scarce. The observational evidence for small-scale distortions in the vertical velocity fields of disk galaxies comes from the so-called *rolling motions* in our Galaxy [observed in the b vs. v (LSR) plots of the H I galactic distribution; Yuan & Wallace 1973; Feitzinger & Spicker 1985], the velocity field of the ionized gas in M51 (Goad, De Veny, & Goad 1979), rotation curves of some spirals (Pismis 1965; Rubin, Ford, & Thonnard 1980), and optical and radio isovelocity maps of some field galaxies (Bosma 1978; Pismis 1986). In particular, the study of the velocity field of the ionized gas in M51 performed by Goad et al. (1979) suggests that part of the observed non-rotational velocities could be due to motions perpendicular to the plane of the disk. Pismis (1965, 1986), on the other hand, has pointed out the relevance of analyzing the location of the velocity undulations in the rotation curve with respect to the spiral structure of the host galaxy. Clearly, all this kinematic information may be important to our understanding of corrugations.

In this paper we report the detection of a corrugated velocity field in the ionized gas of the nearly face-on spiral NGC 5427. The central velocity of the H α emission line shows velocity shifts with similar behavior when the gas passes through the spiral arms. This behavior can be understood as being due to a hydraulic jump, or bore, generated by the interaction of the spiral density wave with the gas of a thick gaseous disk, as discussed by Martos & Cox (1998, hereafter MC) and Martos et al. (1999). The detection of this velocity pattern in NGC 5427 does not answer the current questions about the morphogenesis of corrugations but rep-

¹ Based on observations made with the William Herschel Telescope operated on the island of La Palma by the Isaac Newton Group in the Spanish Observatorio del Roque de Los Muchachos of the Instituto de Astrofísica de Canarias.

² Instituto de Astrofísica de Andalucía (CSIC), Apdo. 3004, 18080 Granada, Spain; emilio@iaa.es, eperez@iaa.es, rosa@iaa.es.

³ Instituto de Astronomía, Universidad Nacional Autónoma de México, Apdo. Postal 70-264, 04510-México DF, México; pepe@astroscu.unam.mx, marco@astroscu.unam.mx.

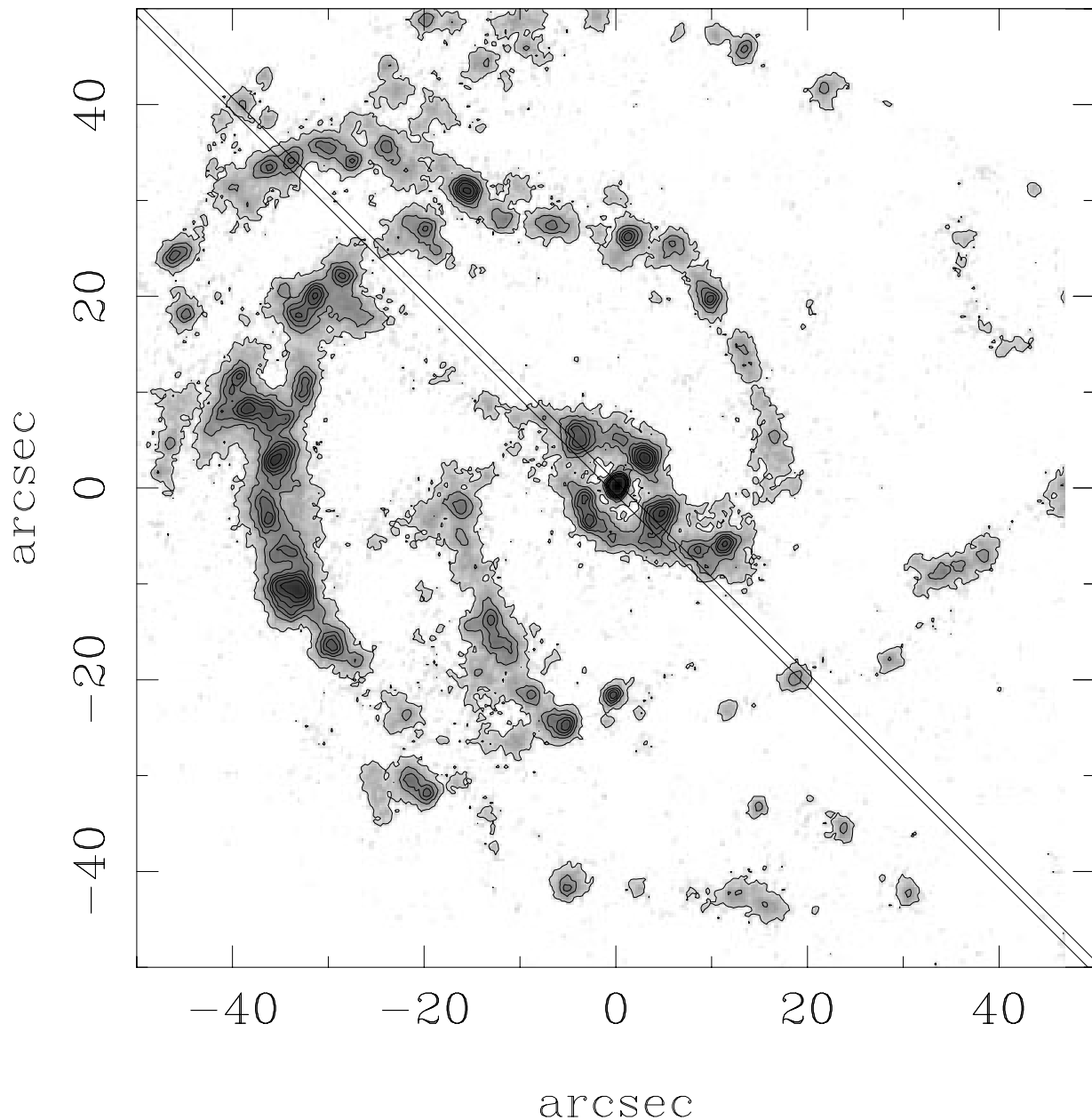


FIG. 1.—Continuum-subtracted H α narrowband CCD image of NGC 5427. North is up and east to the left. The slit used for the spectroscopic observations is drawn for reference at a position angle of 45°.

resents a powerful tool to explore further the theoretical and observational aspects of the problem. The paper has been organized in three sections, the first one being this introduction; § 2 is devoted to the description of the observations and reduction procedure, and, finally, in § 3 we discuss the results and outline the main conclusions.

2. OBSERVATIONS AND DATA REDUCTION

NGC 5427 is a nearly face-on spiral, interacting with the spiral NGC 5426. The two galaxies in this binary system have the same morphological classification, SA(s)c, in the Second Reference Catalogue of Bright Galaxies (de Vaucouleurs, de Vaucouleurs, & Corwin 1976), and they are cataloged as object 276 in the atlas of Arp (1966) and object 21 in the catalog of Vorontsov-Velyaminov (1959). The system has been studied photometrically and spectro-

scopically by Blackman (1982). The inclination of NGC 5427 with respect to the plane of the sky is about 30°, and the position angle for the line of nodes is about 70° (Blackman 1982; Grosbol 1985). The star formation properties of NGC 5427 have been studied by González Delgado & Pérez (1992, 1997) and González Delgado et al. (1997), who have analyzed the H α emission and the luminosity and size distribution functions. The nucleus of NGC 5427 is classified as a Seyfert type 2, and Colina et al. (1997) have studied the relative importance of the circumnuclear star formation and nuclear activity.

The observations were done with the 4.2 m William Herschel Telescope at the Observatorio del Roque de los Muchachos during a director's service night, 1990 March 18. We used the red arm of the ISIS spectrograph with an EEV CCD chip and the grating R600. A spectral range of

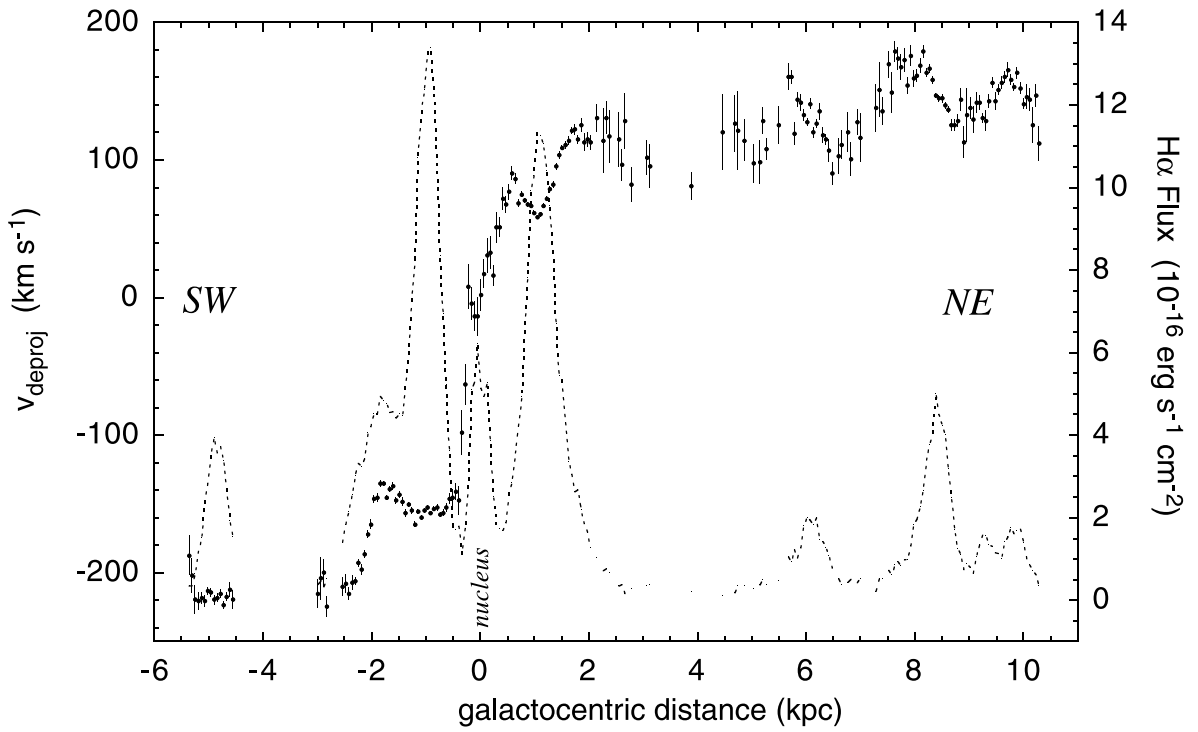


FIG. 2a

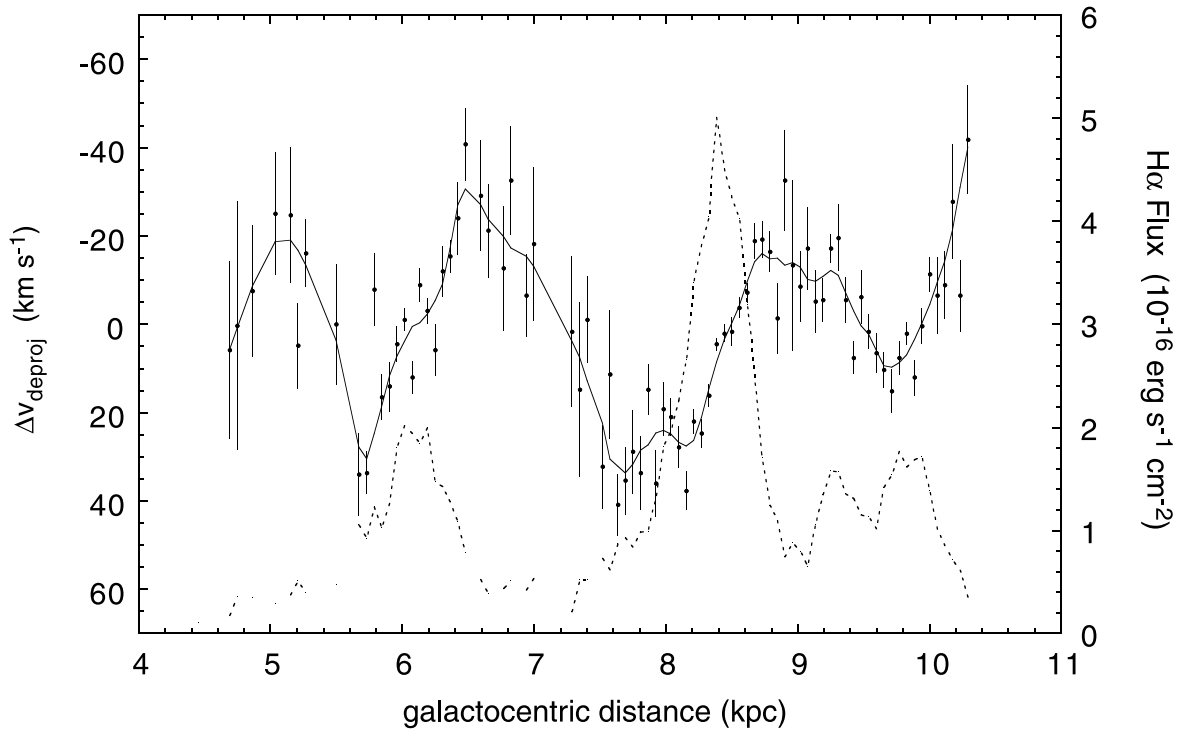


FIG. 2b

FIG. 2.—(a) Velocity (dots with error bars) and intensity (dotted line) curves obtained from the $H\alpha$ emission line along the slit. The velocity (left-hand ordinate scale) has been corrected for the disk inclination (30°) and the P.A. of the line of nodes (70°), and the systemic velocity has been subtracted. The spatial scale is computed with a systemic velocity of 2618 km s^{-1} and $H_0 = 75 \text{ km s}^{-1} \text{ Mpc}^{-1}$. The $H\alpha$ intensity scale is drawn in the right-hand ordinate scale. (b) An expansion of the two curves around the zone between 5 and 10 kpc, where the relationship between the velocity and intensity structures is clearest; the velocity curve has been detrended for the gentle rising slope and plotted upside-down from (a), with the approaching blueshifted velocities higher in the ordinate axis.

900 Å was covered with a dispersion of $0.74 \text{ \AA pixel}^{-1}$, centered at 6560 Å. The sampling along the spatial direction is 0.33 pixel^{-1} , equivalent⁴ to 56 pc pixel^{-1} ; thus, for $H_0 = 75 \text{ km s}^{-1} \text{ Mpc}^{-1}$, the scale is $170 \text{ pc arcsec}^{-1}$. An exposure of 2000 s was secured through a 4' long, 1" wide slit at a position angle of 45° across the nucleus (Fig. 1).

The data were reduced using the FIGARO data processing software. Bias and flat-fielding were performed in the usual way. A two-dimensional wavelength calibration was done using the program ARC2D (Wilkins & Axon 1992) by fitting a third-order polynomial to the position of the lines in the calibration lamp frames; the rms deviation from the fits was less than 0.1 \AA . The FWHM of the sky lines [O I] $\lambda\lambda 6300, 6363$ measured in the wavelength-calibrated frame of NGC 5427 is 1.51 ± 0.06 and $1.57 \pm 0.08 \text{ \AA}$, respectively; thus, the spectral resolution is better than 1.6 \AA . The spectrum was flux-calibrated using a flux standard observed through a very wide slit and the sky background subtracted.

We used the program LONGSLIT (Wilkins & Axon 1992) to interactively perform a Gaussian fit to the emission lines along the slit. The program output includes the position and intensity of the emission lines, together with the respective fitting errors. The rms error in velocity due to the wavelength calibration is 1.3 km s^{-1} , smaller than errors in the Gaussian fit. In the subsequent manipulation of the data, we propagate the errors accordingly. The final errors are shown in Figures 2a and 2b where the main contribution comes from the Gaussian fit uncertainties.

3. RESULTS AND INTERPRETATION

Figure 2a shows the deprojected radial velocity of NGC 5427, V_{deproj} , together with the full intensity curves for the emission line H α along the slit. The velocity curve has been corrected for the galactic systemic motion, the projection with respect to the plane of the sky (30°), and the P.A. of the line of nodes (70°). Our data is more extended toward the northeast, away from the interaction zone with NGC 5426. The southern half of NGC 5427 is significantly affected by the presence of NGC 5426, but, in contrast, the northern half of the galaxy does not show any significant structural perturbation and seems to be relatively undisturbed. Thus, the north-south velocity asymmetries are likely due to the perturbation induced by NGC 5426. The asymmetry in the star-forming properties is also interesting, and it has been discussed by Blackman (1982) and González Delgado & Pérez (1992). The figure shows a remarkably well-defined wavelike structure in the central velocity, superimposed to a gentle rise toward the northeast. Figure 2b shows the variations in the deprojected velocity ΔV_{deproj} (see below), when the slit passes through the three spiral features located at galactocentric distances from 5 to 10 kpc in the northeast. The amplitude of the variations ΔV_{deproj} are in the range ± 20 to $\pm 30 \text{ km s}^{-1}$ for the three main features. In this figure, the velocity has been detrended by fitting a linear component to the gentle rise and is presented upside-down with respect to Figure 2a, so that blueshifted material is seen higher in the velocity axis.

The cross-correlation of the velocity and intensity curves for these three features shows that the peak velocities are displaced from the peak intensities by the same distance in

all three cases. This is shown in Figure 3 (solid line) together with the autocorrelations for the velocity (dotted line) and intensity (dashed line) curves; a negative lag indicates a shift toward smaller galactocentric distances. The FWHM of the autocorrelation functions is 560 pc for the intensity and 910 pc for the velocity. The velocity versus intensity cross-correlation function is slightly asymmetrical, with a peak at 300 pc and a full width at zero intensity centroid at 500 pc. Thus, the displacement between the peak velocities and the arm peak intensities amounts to about one-half of the arm width.

An inspection of the Wide Field Planetary Camera 2 (WFPC2) image from the *Hubble Space Telescope* (HST) archive, taken through the F606W filter (Fig. 4), shows the location of the dust lanes along the spiral arms. In the central regions (inside $r \sim 25''$), the dust lanes are located in the concave (interior) side of the spiral arms. For the regions external to $25''$, however, the position of the dust lanes depends on the interaction with NGC 5426. For the northeast region, which is relatively unperturbed and where the residual velocity curve is better defined, the dust lanes are clearly located in the convex (exterior) side of the arms. In contrast, the heavily perturbed southwest region displays a different pattern, and, even as far as $50''$ away the center, the dust lanes appear in the concave (interior) side of the arm. These north-south asymmetries, as stated above, are due to the velocity perturbations induced by NGC 5426, and the corotation radius cannot be defined in a unique form in this galaxy. For the purposes of the present study, however, we restrict the analysis to the relatively unperturbed northeast region and use the location of the dust lanes to infer the direction of gas flow through the arms.

The wavy structure of ΔV_{deproj} represents the projection of the residual galactic velocity on the line of sight, once corrected from systemic and rotational velocities. The system velocity has been estimated at the position of the maximum emission at the core. The variable ΔV_{deproj} can be written in terms of the inclination angle, i , and the angle between the position vector and the line of nodes, ϕ , as

$$\Delta V_{\text{deproj}} = \Delta V_{\perp} \cos i + \Delta V_{\parallel} \sin i, \quad (1)$$

and assuming that the parallel component is only due to rotation,

$$\Delta V_{\text{deproj}} = \Delta V_{\perp} \cos i + r\Delta\Omega \sin i \cos \phi, \quad (2)$$

where r is the galactocentric radius, V_{\perp} is the vertical velocity component, and Ω is the angular rotation speed in the local galactic frame. According to this expression, there are three main factors (or any combination of them) that could be producing the undulation of the residual velocity: (1) The galactic disk is not planar, and i changes with galactocentric radius. (2) The galaxy has a corrugated vertical velocity component. (3) The rotation curve of the gas is accelerated and decelerated in a cyclic way. The inclination of NGC 5427 ($\sim 30^\circ$) is small enough to place vertical motions nearly on the line of sight and yet large enough to exhibit the rotational motions. From the second term in equation (2), and even when a good fraction of the velocity corrugation is likely vertical, one cannot discard the presence of velocity components parallel to the disk.

Figure 2b shows that the approaching (negative values) peaks in ΔV_{deproj} occur in the convex border of the arms, whereas the receding maxima (positive values) are located behind the H α emission maxima, in the concave side. An

⁴ According to the NED IPAC Database, we adopt a recession velocity of 2618 km s^{-1} for NGC 5427.

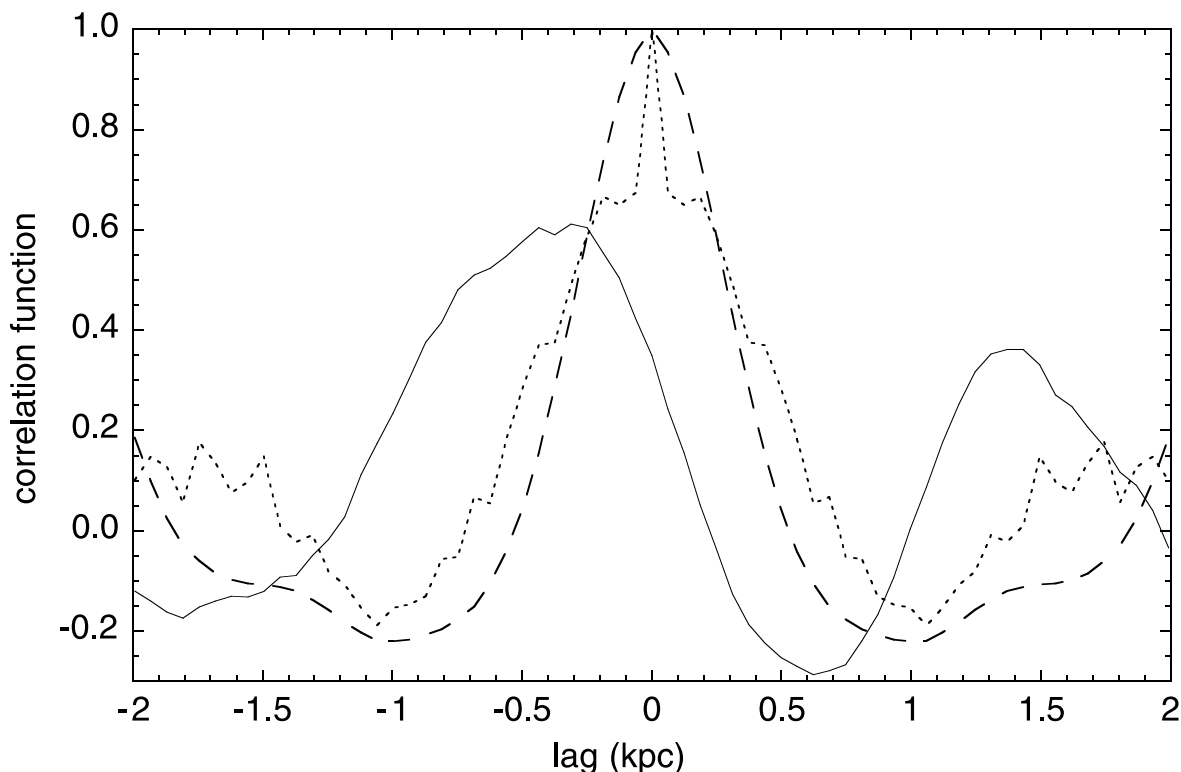


FIG. 3.—Cross-correlation function (*solid line*) of the two curves shown in Fig. 2*b*. The velocity (*dotted line*) and intensity (*dashed line*) autocorrelation functions are also plotted. The two central pixels of the velocity autocorrelation function are produced by noise and should not be taken into account; notice then how the velocity autocorrelation is significantly wider than the intensity.

approaching velocity means that the gas either is flowing up to higher galactic latitudes or the rotation velocity is decelerating. On the other hand, the receding velocities indicate that the gas is either falling down onto the galactic plane or is accelerating. Given that the FWHM of the velocity autocorrelation function is almost twice the FWHM of the $H\alpha$ intensity autocorrelation, it seems as if the gas flow is decelerating and jumping above the arm and depositing material in the concave side. This behavior is similar to the response of a gas flow into a spiral density wave in a thick and magnetized gaseous disk, as recently discussed by MC. They found that the gas entering a spiral arm rises suddenly on the upstream side of the arm then accelerates and bends downward, finally landing on a large downfall region downstream of the arm. Figure 5 illustrates this dynamical behavior for case 28 of MC, in which the radial extent of the arm is 1 kpc. The center of the horizontal axis, $x = 0$, corresponds to the minimum of the potential well, z is the vertical distance above the midplane, and the magnetic field is oriented perpendicular to the x - z plane, along the long axis of the arm. The upstream ascent and downstream downfall of the gas above the arm are so predicted by the model in this numerical MHD simulation.

This scenario fits quite well the phenomenology that we find in NGC 5427. The observed deprojected velocity amplitudes are of the same order as the ones found by MC. Figure 5 shows that one should expect that the approaching velocity maxima would appear in the upstream side of the arms; for NGC 5427, these maxima are located in the convex borders. Thus, if the observed velocity pattern is induced by a spiral density wave, the gas is entering the arm through the convex side, which can only occur outward of

the corotation radius in a trailing arm. This is supported by the geometrical arguments described above. Thus, the main features observed in the radial corrugated velocity pattern seem to be explained by the perturbations originated in the velocity field pattern of gas encountering a spiral arm. Such a velocity field occurs on both sides of the galactic midplane, generating doubled emission lines. The relative strengths of these two components depend on the relative position of the gas centroid with respect to the center of the spiral potential minimum, but the extinction through the disk and the low emissivity of gas in the interarm regions can make it difficult to detect, or separate, the emission generated on the far side of the disk. The optical thickness of spiral galaxies is highly variable across the disk; it is optically thin in most parts of the interarm regions and much more opaque along the arms, particularly in the dust patches (see, e.g., Disney, Davies, & Philipps 1989; Marziani et al. 1999). Our spectroscopic data passing through the three spiral features of the northeast region could reach visual extinctions between 1 and 4 mag (Marziani et al. 1999). At present we cannot provide specific extinction values along the arms, but it is possible that the $H\alpha$ emission generated at the back side is below our detection limit. The opacity in the interarm regions is certainly much lower, but the emissivity of the ionized gas is also much smaller, and the signal-to-noise ratio is accordingly lower. Nonetheless, there is a hint that we may be detecting some of the far-side emission because the FWHM of the emission lines increases in the high-velocity features. Figure 6 shows that the emission with $|\Delta V| > 10 \text{ km s}^{-1}$ has larger dispersion values, but the low signal-to-noise ratio prevents us from discerning between foreground and background velocity

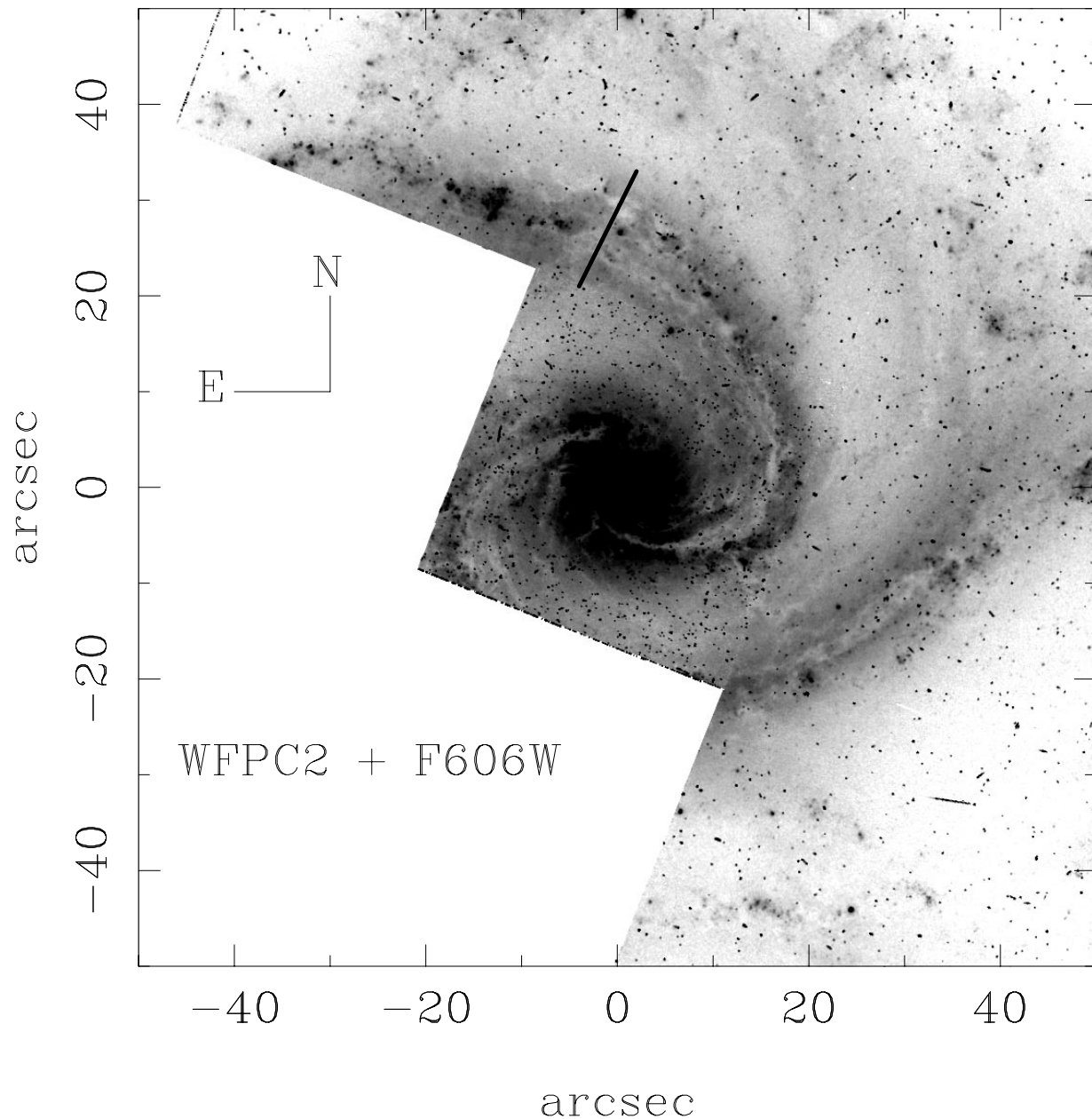


FIG. 4.—Image of NGC 5427 taken with the WFPC2 through the F606W filter. The location of dust lanes is apparent as white patches running along the spiral arms. The line segment marked in the main north spiral arm shows the position at which the dust lanes change from the internal (concave) side to the external (convex) border. Our analysis is done in the outer regions of the northeast part of the spiral structure, where the dust lane is located in the convex side of the arm.

peaks (we thank the referee for pointing out this possibility). More work with higher quality data is needed to resolve this issue conclusively.

Even though the galactic bore model seems to provide a very appealing explanation to the observed velocity corrugations in NGC 5427, other mechanisms could also be inducing or enhancing the corrugations of the velocity field. The fact that this galaxy is a member of an interacting pair, whose companion has a mass similar to or larger than NGC 5427, makes it likely that the perturbations originated by the tidal interaction largely will affect the velocity field, producing corrugated patterns (Edelsohn & Elmegreen 1997). In addition, the azimuthal corrugations in the arms originated by magneto-gravitational instabilities (J. Franco

et al. 2001, in preparation) also must be present and superimposed with the other deviations of the velocity field. We notice, however, that the velocity field resulting from the Parker instability will be essentially that of a downfall (toward the midplane) along the bent magnetic field lines and not the rising and falling motions expected from the galactic bore picture.

Summarizing, here we report the detection of a corrugated velocity pattern in the disk of NGC 5427. A detailed analysis of this velocity structure shows a remarkably good qualitative agreement between the observed features and those derived from the galactic bore model described by MC and Martos et al. (1999). Given that the only requirements for this mechanism to work are the existence of a

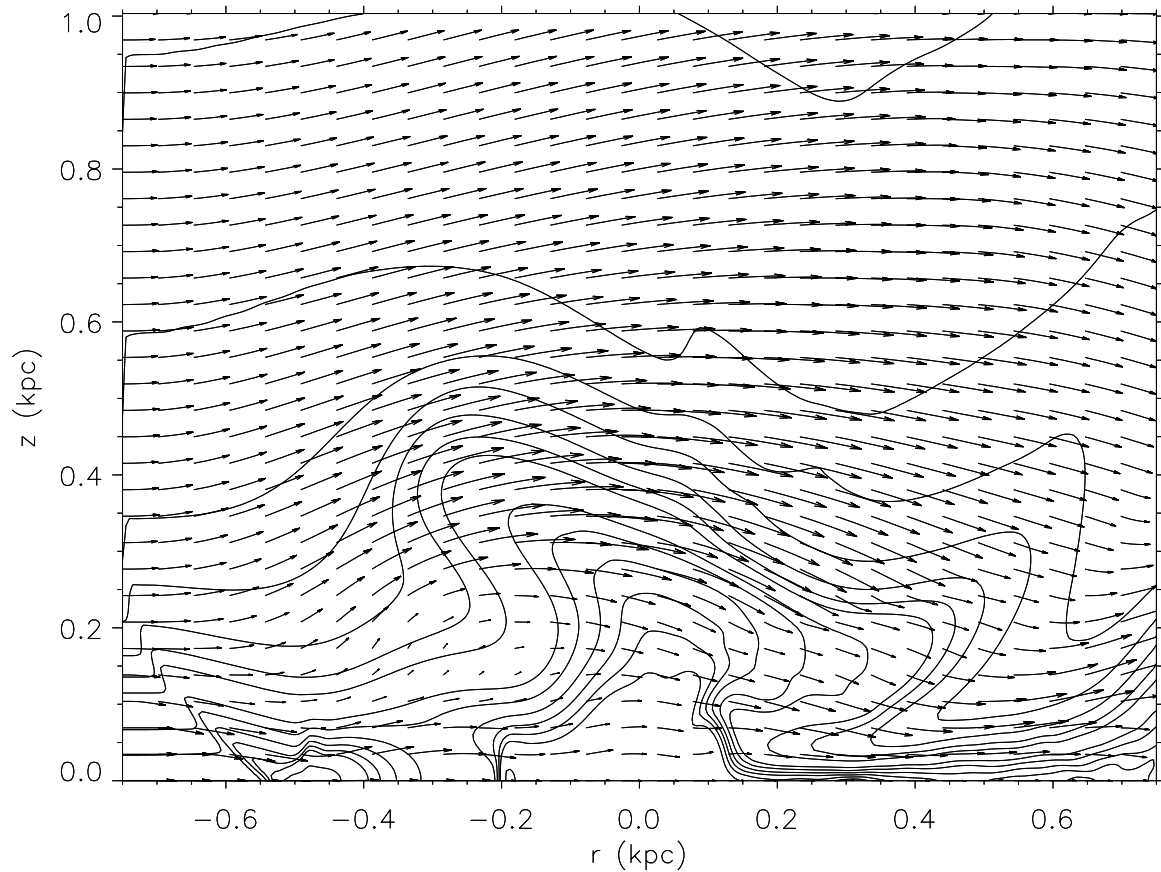


FIG. 5.—Density contours (15 levels, from 0.01 to 3 times the initial midplane density) and velocity field for gas approaching a spiral arm from the left-hand (upstream) side of the numerical grid, case 28 of MC at an elapsed time of 67 Myr. The size of the longer velocity vector in the field corresponds to a speed of 55 km s^{-1} .

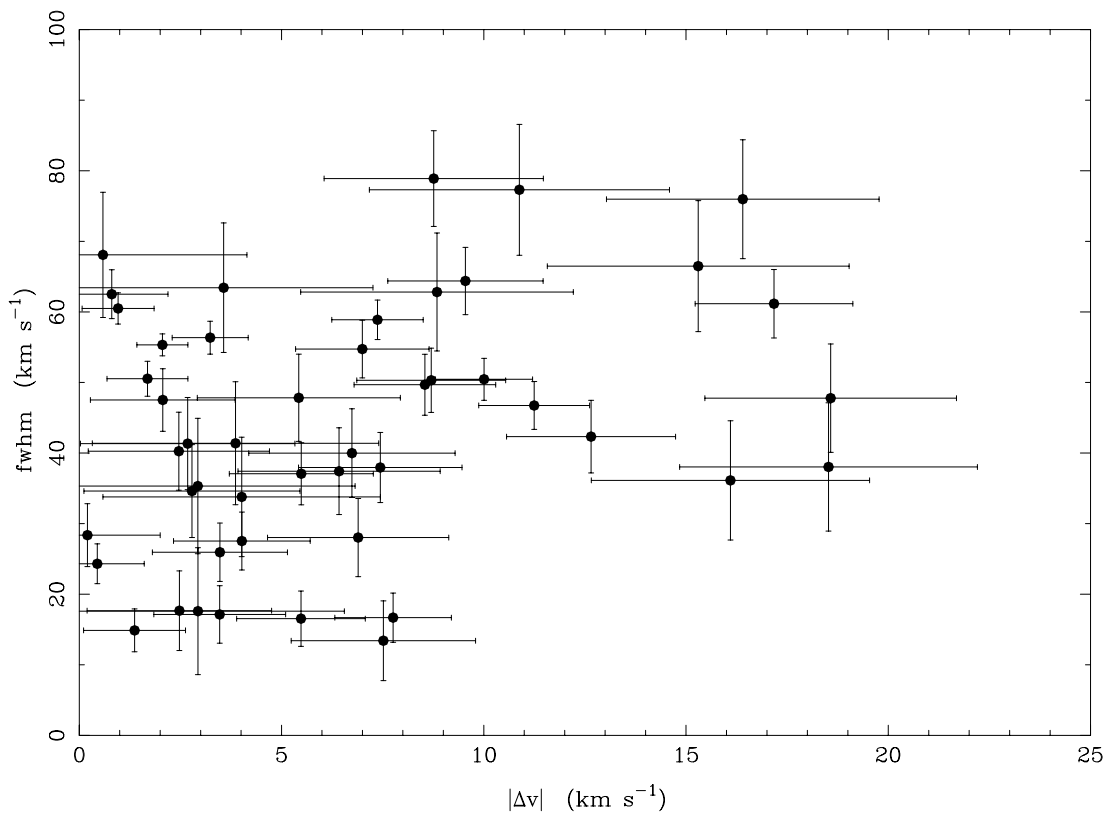


FIG. 6.—Line widths (FWHM) vs. $|\Delta V|$ for the spectral features used to determine the velocity curve. Note how for $|\Delta V| \geq 10 \text{ km s}^{-1}$ the FWHM of the lines is always larger than 35 km s^{-1} . This widening could be originated by the blending of two unresolved features coming from both sides of the galaxy.

spiral density wave and a magnetic field (with a strength similar to those observed in our Galaxy; see MC and discussion therein), the generation of radial velocity corrugations must be a common occurrence in spiral galaxies. The search for vertical velocity corrugations in a sample of face-on galaxies is now a must follow-up program. The difference with the previous situation is that now we know how and what to search for.

We thank Don Cox for helpful discussions and Arcadio Poveda for pointing out the early works of Paris Pismis on undulations of the rotation curves of spirals. We are indebted to an anonymous referee for a very useful and detailed report that helped us to improve the contents of the paper. We are grateful to Dave L. King who made the spectroscopic observations in service mode. This research has made use of the Starlink Software Collection of the UK

PPARC and of the NASA/IPAC Extragalactic Database (NED), which is operated by the Jet Propulsion Laboratory, California Institute of Technology, under contract with the National Aeronautics and Space Administration. The *HST* image of NGC 5427 was retrieved from the Space Telescope European Coordinating Facility *HST* archive. E. J. A. acknowledges financial support granted by CONACYT-México and CSIC-Spain under the agreement of both institutions; his work is partially supported by the Spanish DGICYT through grants PB97-1438-C02-02 and by the Research and Education Council of the Autonomous Government of Andalucía (Spain). E. P. and R. M. G. D. are supported by Spanish DGICYT grant PB98-0521. J. F. thanks the Instituto de Astrofísica de Andalucía for its warm hospitality and acknowledges partial support by DGAPA-UNAM grant IN130698 and by an R&D CRAY Research grant.

REFERENCES

- Alfaro, E. J., Cabrera-Caño, J., & Delgado, A. J. 1992a, *ApJ*, 399, 576
 ———. 1992b, in IAU Symp. 149, *The Stellar Populations of Galaxies*, ed. B. Barbuy & A. Renzini (Dordrecht: Kluwer), 386
 Arp, H. C. 1964, *ApJ*, 139, 1045
 ———. 1966, *Atlas of Peculiar Galaxies* (Pasadena: Caltech)
 Berdnikov, L. N., & Efremov, Yu. N. 1993, *Astron. Lett.*, 19, 389
 Blackman, C. P. 1982, *MNRAS*, 200, 407
 Bosma, A. 1978, Ph.D. thesis, Univ. Groningen
 Colina, L., García-Vargas, M. L., González Delgado, R. M., Mas-Hesse, J. M., Pérez, E., Alberdi, A., & Krabbe, A. 1997, *ApJ*, 488, L71
 de Vaucouleurs, G., de Vaucouleurs, A., & Corwin, H. 1976, *Second Reference Catalogue of Bright Galaxies* (Austin: Univ. Texas Press)
 Disney, M. J., Davies, J. I., & Philipps, S. 1989, *MNRAS*, 239, 939
 Dixon, M. E. 1967, *MNRAS*, 137, 337
 Edelson, D. J., & Elmegreen, B. G. 1997, *MNRAS*, 287, 947
 Feitzinger, J. V., & Spicker, J. 1985, *MNRAS*, 214, 539
 Florido, E., Battaner, E., Prieto, M., Mediavilla, E., & Sánchez-Saavedra, M. L. 1991, *MNRAS*, 251, 193
 Franco, J., Tenorio-Tagle, G., Bodenheimer, P., Rozyczka, M., & Mirabel, I. F. 1988, *ApJ*, 333, 826
 Goad, J. W., De Veny, J. B., & Goad, L. E. 1979, *ApJS*, 39, 439
 Gómez de Castro, A. I., & Pudritz, R. E. 1992, *ApJ*, 395, 501
 González Delgado, R. M., & Pérez E. 1992, in *ASP Conf. Ser.*, 31, *Relationships between Active Galactic Nuclei and Starbursts Galaxies*, ed. A. V. Filippenko (San Francisco: ASP), 371
 ———. 1997, *ApJS*, 108, 199
 González Delgado, R. M., Pérez, E., Tadhunter, C., Vilchez, J. M., & Rodríguez-Espinosa, J. M. 1997, *ApJS*, 108, 155
 Grosbol, P. J. 1985, *A&AS*, 60, 261
 Gum, C. S., Kerr, F. J., & Westerhout, G. 1960, *MNRAS*, 121, 132
 Kerr, F. J. 1957, *AJ*, 62, 93
 Kim, J., Hong, S. S., & Ryu, D. 1997, *ApJ*, 485, 228
 Lockman, F. J. 1977, *AJ*, 82, 408
 Malhotra, S. 1995, *ApJ*, 448, 138
 Martos, M., Allen, C., Franco, J., & Kurtz, S. 1999, *ApJ*, 526, L89
 Martos, M., & Cox, D. P. 1998, *ApJ*, 509, 703 (MC)
 Marziani, P., D'Onofrio, M., Dultzin-Hacyan, D., & Sulentic, J. W. 1999, *AJ*, 117, 2736
 Nelson, A. H. 1976, *MNRAS*, 177, 265
 ———. 1985, *MNRAS*, 215, 161
 Parker, E. N. 1966, *ApJ*, 145, 811
 Pismis, P. 1965, *Bol. Obs. Tonantzintla Tacubaya*, 4, 8
 ———. 1986, *Rev. Mexicana Astron. Astrofis.*, 12, 79
 Rubin, V. C., Ford, W. K., & Thonnard, N. 1980, *ApJ*, 238, 471
 Sanders, D. B., Solomon, P. M., & Scoville, N. Z. 1984, *ApJ*, 276, 182
 Santillán, A., Franco, J., Martos, M., & Kim, J. 1999, *ApJ*, 515, 657
 Santillán, A., Kim, J., Franco, J., Martos, M., Hong, S. S., & Ryu, D. 2000, *ApJ*, 545, 353
 Spicker, J., & Feitzinger, J. V. 1986, *A&A*, 163, 43
 Vorontsov-Velyaminov, B. A. 1959, *Atlas and Catalogue of Interacting Galaxies* (Moscow: Sternberg Institute)
 Weinberg, M. D. 1991, *ApJ*, 373, 391
 Wilkins, T. N., & Axon, D. J. 1992, in *ASP Conf. Ser.* 25, *Astronomical Data Analysis Software and Systems I*, ed. D. M. Worrall, C. Biemesderfer, & J. Barnes (San Francisco: ASP), 427
 Yuan, C., & Wallace, L. 1973, *ApJ*, 185, 453